Scientia Iranica D (2014) 21(3), 904–923

SCIENTIA IRANICA

Sharif University of Technology

Scientia Iranica

Transactions D: Computer Science & Engineering and Electrical Engineering

www.scientiairanica.com

A new algorithm for three-phase power transformer differential protection considering effect of ultra-saturation phenomenon

B. Noshad*, **M. Razaz**, **S.Gh. Seifossadat**

Department of Electrical Engineering, Shahid Chamran University of Ahvaz, Ahvaz, Iran.

Received 27 February 2013; received in revised form 27 May 2013; accepted 18 June 2013

KEYWORDS
Three-phase power transformer differential protection;
Ultra-saturation phenomenon;
Magnetic inrush current;
Internal faults;
External faults;
False trip;
Harmonic components;
Differential current.

Abstract. A transient phenomenon that leads to the false trip of the power transformer differential protection during the energization of a loaded power transformer is the ultra-saturation phenomenon. In this paper, at first, a new algorithm for three-phase power transformer differential protection, considering the effect of the ultra-saturation phenomenon, is presented. To model the ultra-saturation phenomenon, the nonlinear characteristic of the transformer core and the effect of saturation of the current transformers are taken into account. It is assumed that the load of the transformer is resistive and inductive. In this algorithm, the ultra-saturation phenomenon, external and internal faults of the power transformer and magnetic inrush current are simulated, and appropriate criteria using the signal harmonic components of the differential current will be presented for the Discrete Fourier Transform (DFT) algorithm to distinguish between. In this paper, simulation is done by PSCAD and MATLAB programs.

1. Introduction

The differential relay of power transformers is the most important part of power systems [1]. Magnetizing inrush current in the power transformer is a transient phenomenon that can cause the false trip of the transformer differential protection, as when a power transformer is switched on, it can be much higher than its nominal value and, hence, may cause the false trip of the differential protections [1-2]. Normally, in order to distinguish between external faults, internal faults and magnetizing inrush current, an algorithm is used in which the differential protection operates when the amplitude of the basic component of the differential current is fixed higher than 0.25 p.u and the level of the second harmonic to the basic harmonic of the differential current fixes lower than 15% [3-7]. However, it has been shown that under certain conditions, the false trip of differential protection under magnetizing inrush current has lead to the tripping of healthy transformers [3-5]. When a loaded power transformer is switched on, it may cause a status called the nominated ultra-saturation phenomenon. In this case, the DC flux in the magnetic core of the power transformer at the primary stage of the process increases rather than decreases [3]. Hence, the amplitude of the basic component of the differential current gets higher and the level of the second harmonic decreases lower than the level of the relay restrain [3-5]. For analytical study of the ultra-saturation phenomenon,

*. *Corresponding author. Tel: +98 611 3330015; Fax: +98 611 3330016*
E-mail addresses: bahramnoshad@yahoo.com (B. Noshad); razaz_m@scu.ac.ir (M. Razaz); seifossadat@yahoo.com (S.Gh. Seifossadat)

an initial loaded power transformer energization model was suggested and the false trip of the differential protection has been described using this model, [3-5]. In [3], many simplifications during the simulations are carried out, which take the magnetizing reactance of the time-variant characteristic as an equivalent inductance, neglecting the core model of the power transformer, without considering the transferring effect of the current transformer to the primary inrush, and only considering the resistive load, which does not coincide with real situations. Weng et al. revised their previous model in 2007. According to them, the previous model cannot be used to study the ultra-saturation phenomenon. So, a new model for studying the ultra-saturation phenomenon during loaded power transformer energization is proposed with the current transformer model, including the effect of the magnetic hysteresis and the nonlinear magnetizing reactance, not only the resistive load [4]. But in [4], the core losses of the power transformer are neglected and a difficult model for the current transformer in the primary side is considered whose main difficulty in current transformer modeling is the hysteresis loop simulation. Wiszniewski et al. illustrated the conditions which must be discovered to make ultra-saturation and excessive ultra-saturation possible in 2008 [5]. The ATP-EMTP program is used for simulation. For determining the conditions that discovered the ultra-saturation and excessive ultra-saturation phenomenon in [5], the core model of the power transformer and the magnetizing reactance are ignored, which does not correspond with the real status. In all previous studies of ultra-saturation phenomenon, the model of a loaded power transformer was considered as single-phase and an appropriate protection algorithm had not been described for preventing the false trip of differential protection due to the ultra-saturation phenomenon [3-5]. Several studies have been done to distinguish internal faults from external faults and magnetic inrush current using various algorithms, such as wavelet transform [8,9], the fuzzy technique [10,11], the neural network [12,13], combined wavelet transform and neural network [14], harmonic restraint [15] and park transform [16]. Also, some work has used special algorithms, such as short-time correction transform [17], the support vector machine-based protection scheme [18], self adaptive transformer differential protection [19], time-domain analysis of the differential power signal [20], an inner bridge connection [21], standard 87T differential protection for a power transformer and a special power transformer [22,23] and intelligent hybrid systems [24] to distinguish between the transient phenomena. But, in all these studies, the ultra-saturation phenomenon was not taken into account.

In this paper, at first, a new model for investigating the ultra-saturation phenomenon during the energization of a loaded three-phase power transformer is presented. To model the ultra-saturation phenomenon, the nonlinear characteristic of the transformer core and the saturation effect of current transformers are taken into account. It is assumed that the load of the transformer is a resistive and inductive load. Also, a new model is presented for the current transformer which is very simple and effective. In addition to a new model for the power transformer and the current transformer, in this paper, a new algorithm for three-phase power transformer differential protection, considering the effect of the ultra-saturation phenomenon, is presented. In this algorithm, the ultra-saturation phenomenon, power transformer external faults (including three-phase fault, three-phase-to-ground fault, phase-to-ground fault, phase-to-phase fault, and phase-to-phase-to-ground fault), power transformer internal faults (including turn-to-ground fault, turn-to-turn fault, and phase-to-phase fault), and magnetic inrush current are simulated, and appropriate criteria using signal harmonic components of the differential current to distinguish between these phenomenon using the DFT algorithm will be presented. The differential protection of the power transformer must be fast and accurate, so the description and control of the ultra-saturation phenomenon are necessary for preventing the false trip of the differential protection. In this paper, simulation is done by PSCAD and MATLAB programs.

2. Ultra-saturation modeling

2.1. Modeling of loaded three-phase transformer energization

The modeling of power transformers is always done using both magnetic and electrical circuits. The basic structure of a three-phase, two-winding, three-legged power transformer is shown in Figure 1(a); Figure 1(b) shows the magnetic equivalent circuit of the transformer shown in Figure 1(a). According to

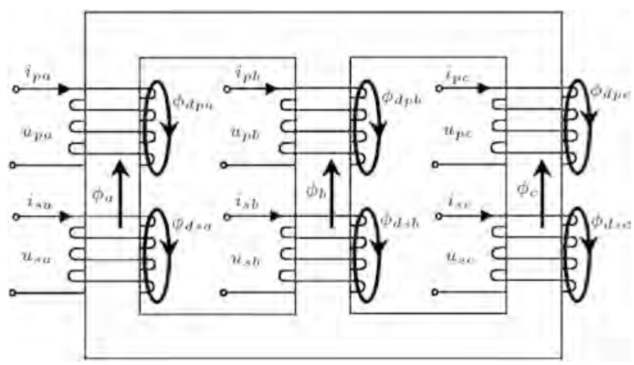

Figure 1a. The basic structure of a three-phase, two-winding, three-legged power transformer.

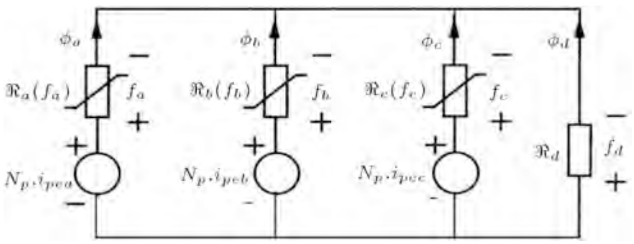

Figure 1b. The magnetic equivalent circuit of three-phase transformer.

Figure 1(b):

$$-N_p i_{pea} + f_a - \Re_d \phi_d = 0, \tag{1}$$

$$-N_p i_{peb} + f_b - \Re_d \phi_d = 0, \tag{2}$$

$$-N_p i_{pec} + f_c - \Re_d \phi_d = 0, \tag{3}$$

$$\phi_a + \phi_b + \phi_c + \phi_d = 0. \tag{4}$$

By considering the saturation curve, reluctances a, b, and c in Figure 1(b) are nonlinear and defined as follows [25]:

$$\Re_a(f_a)^{-1} = \frac{k_{1a}}{\left(1 + \left(\frac{|f_a|}{f_{0a}}\right)^{p_a}\right)^{\frac{1}{p_a}}} + k_{2a}, \tag{5}$$

$$\Re_b(f_b)^{-1} = \frac{k_{1b}}{\left(1 + \left(\frac{|f_b|}{f_{0b}}\right)^{p_b}\right)^{\frac{1}{p_b}}} + k_{2b}, \tag{6}$$

$$\Re_c(f_c)^{-1} = \frac{k_{1c}}{\left(1 + \left(\frac{|f_c|}{f_{0c}}\right)^{p_c}\right)^{\frac{1}{p_c}}} + k_{2c}. \tag{7}$$

According to Figure 1(b):

$$f_a = \Re_a(f_a).\phi_a, \tag{8}$$

$$f_b = \Re_b(f_b).\phi_b, \tag{9}$$

$$f_c = \Re_c(f_c).\phi_c. \tag{10}$$

Due to Eqs. (5)-(10):

$$\phi_a = \left(\frac{k_{1a}}{\left(1 + \left(\frac{|f_a|}{f_{0a}}\right)^{p_a}\right)^{\frac{1}{p_a}}} + k_{2a}\right).f_a, \tag{11}$$

$$\phi_b = \left(\frac{k_{1b}}{\left(1 + \left(\frac{|f_b|}{f_{0b}}\right)^{p_b}\right)^{\frac{1}{p_b}}} + k_{2b}\right).f_b, \tag{12}$$

$$\phi_c = \left(\frac{k_{1c}}{\left(1 + \left(\frac{|f_c|}{f_{0c}}\right)^{p_c}\right)^{\frac{1}{p_c}}} + k_{2c}\right).f_c. \tag{13}$$

According to the fact that most three-phase power transformers are connected as a YN/d connection, the electric equivalent circuit can be shown in Figure 2. According to Figure 2, the following equations are presented:

$$u_{pa} = R_p i_{pa} + L_{dp}\frac{di_{pa}}{dt} + N_p\frac{d\phi_a}{dt}, \tag{14}$$

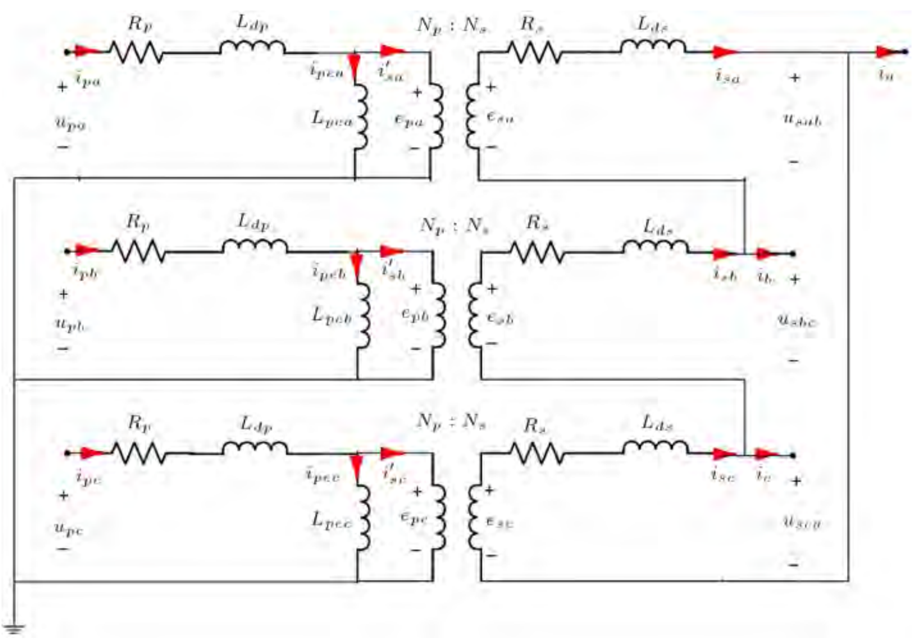

Figure 2. The electric equivalent circuit of a Wye to ground-delta transformer.

$$u_{pb} = R_p i_{pb} + L_{dp}\frac{di_{pb}}{dt} + N_p\frac{d\phi_b}{dt}, \tag{15}$$

$$u_{pc} = R_p i_{pc} + L_{dp}\frac{di_{pc}}{dt} + N_p\frac{d\phi_c}{dt}, \tag{16}$$

$$u_{sab} = -R_s i_{sa} - L_{ds}\frac{di_{sa}}{dt} + N_s\frac{d\phi_a}{dt}, \tag{17}$$

$$u_{sbc} = -R_s i_{sb} - L_{ds}\frac{di_{sb}}{dt} + N_s\frac{d\phi_b}{dt}, \tag{18}$$

$$u_{sca} = -R_s i_{sc} - L_{ds}\frac{di_{sc}}{dt} + N_s\frac{d\phi_c}{dt}. \tag{19}$$

For simulating the ultra-saturation phenomenon, the three-phase power transformer is loaded and it is assumed that the balanced three-phase load of the power transformer is resistive and inductive. By connecting the complex load ($R_b - L_b$) in Wye form to the equivalent circuit of the three-phase power transformer in Figure 2, and based on Kirchhoff voltage and current laws in the secondary side, the following equations can be written:

$$u_{sab} = R_b i_a + L_b\frac{di_a}{dt} - R_b i_b - L_b\frac{di_b}{dt}, \tag{20}$$

$$u_{sbc} = R_b i_b + L_b\frac{di_b}{dt} - R_b i_c - L_b\frac{di_c}{dt}, \tag{21}$$

$$u_{sca} = R_b i_c + L_b\frac{di_c}{dt} - R_b i_a - L_b\frac{di_a}{dt}, \tag{22}$$

$$i_a = i_{sa} - i_{sc}, \tag{23}$$

$$i_b = i_{sb} - i_{sa}, \tag{24}$$

$$i_c = i_{sc} - i_{sb}. \tag{25}$$

Due to Eqs. (17)-(25):

$$\begin{aligned} -R_s i_{sa} - L_{ds}\frac{di_{sa}}{dt} + N_s\frac{d\phi_a}{dt} &= R_b(i_{sa} - i_{sc}) \\ &+ L_b\frac{d(i_{sa} - i_{sc})}{dt} - R_b(i_{sb} - i_{sa}) \\ &- L_b\frac{d(i_{sb} - i_{sa})}{dt}, \end{aligned} \tag{26}$$

$$\begin{aligned} -R_s i_{sb} - L_{ds}\frac{di_{sb}}{dt} + N_s\frac{d\phi_b}{dt} &= R_b(i_{sb} - i_{sa}) \\ &+ L_b\frac{d(i_{sb} - i_{sa})}{dt} - R_b(i_{sc} - i_{sb}) \\ &- L_b\frac{d(i_{sc} - i_{sb})}{dt}, \end{aligned} \tag{27}$$

$$\begin{aligned} -R_s i_{sc} - L_{ds}\frac{di_{sc}}{dt} + N_s\frac{d\phi_c}{dt} &= R_b(i_{sc} - i_{sb}) \\ &+ L_b\frac{d(i_{sc} - i_{sb})}{dt} - R_b(i_{sa} - i_{sc}) \\ &- L_b\frac{d(i_{sa} - i_{sc})}{dt}. \end{aligned} \tag{28}$$

Also, according to Figure 2:

$$\begin{aligned} i_{pa} &= i_{pea} + (N_s/N_p)i_{sa}, \\ i_{pb} &= i_{peb} + (N_s/N_p)i_{sb}, \\ i_{pc} &= i_{pec} + (N_s/N_p)i_{sc}. \end{aligned} \tag{29}$$

In Eqs. (1)-(29) and Figures 1-3, u_{pa}, u_{pb}, u_{pc}, u_{sab}, u_{sbc}, u_{sca}, i_{pa}, i_{pb}, i_{pc}, i_a, i_b and i_c are the voltages and currents of the primary and secondary windings. R_p, R_s, L_{dp} and L_{ds} are the resistance and inductance of the primary and secondary windings. ϕ_a, ϕ_b, ϕ_c and ϕ_d are the flux of the core magnetic through the winding legs and air branch. N_p and N_s are the primary and secondary windings turn. e_{pa}, e_{pb}, e_{pc}, e_{sa}, e_{sb} and

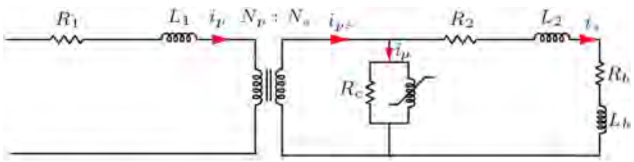

Figure 3a. The current transformer model.

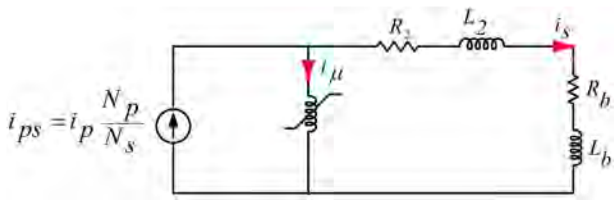

Figure 3b. The current transformer model referred to as secondary side.

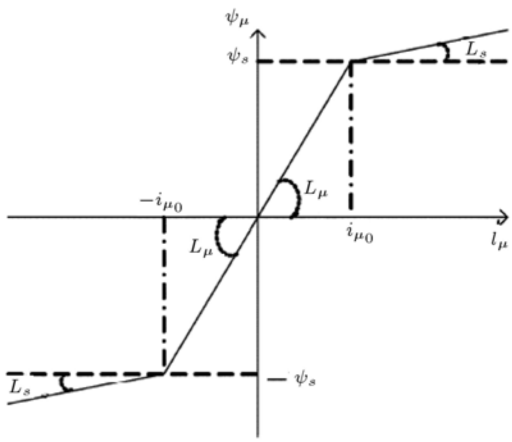

Figure 3c. The magnetizing characteristic of transformer core.

e_{sc} are the inducted primary and secondary voltages of winding legs. f_a, f_b, f_c and f_d are the magnetic potential through the three-legged and air branch. p_a, p_b, p_c, k_{1a}, k_{1b}, k_{1c}, k_{2a}, k_{2b}, k_{2c}, f_{0a}, f_{0b} and f_{0c} are related to the transformer saturation curve, and R_b and L_b are resistive and inductive load of the power transformer.

2.2. Current transformer modeling

In this paper, a new simple and effective model is presented for the current transformer. The current transformer equivalent circuit and the current transformer equivalent circuit referred to in the secondary side are shown in Figures 3(a) and 3(b). In these circuits, R_1 and L_1 are the resistive and inductive components of the equivalent impedance, comprised of the system impedance and leakage impedance of the transformer primary winding; R_2 and L_2 are the resistive and inductive winding of the secondary side of the current transformer; and R_b and L_b are the resistive and inductive burden of the current transformer. To explain the current transformer model in this paper, an appropriate model is developed to predict the transient behavior of a current transformer with a burden consisting of inductance and resistance, taking saturation into account. To model the current transformer, Figures 3(a) and 3(b) are considered. Since the core loss does not affect the behavior of the current transformer saturation, it is neglected [26]. Although the hysteresis effect is not taken into account in this proposed model, but is considered by the IEEE Power System Relaying Committee (IPSR), both results are in good agreement. The main advantages of this proposed model are as follows:

1. Information concerning the B-H curve for the magnetic branch is not required.
2. The hysteresis effect is not taken into account and the results of the proposed model can be compared with the IEEE model considering the hysteresis effect.
3. It involves proper computing speed and accuracy.

If fault occurs in the primary winding of the current transformer and the fault current passes through the primary winding, the core flux increases due to the asymmetrical component. So, the current transformer core approaches the saturation region and this leads to a secondary current distortion. Therefore, an effective current transformer model for protection systems is required, and, in this paper, a very simple and effective model for a current transformer is presented. The accurate curve of the magnetizing curve should be shown as multi-valued if taking hysteresis into account. For the convenience of solving the differential equations, the magnetization curve can be simplified, as shown in Figure 3(c). We suppose that the saturation point is (i_{μ_0}, ψ_s). The inductance inside and outside the saturation regions are L_s and L_μ, respectively. It should be emphasized that the inductance of the magnetizing branch of the transformer is still nonlinear, even if the above-mentioned simplification is used. In most papers, in the linear region of the approximate curve, the magnetization current is considered zero, but, in this model, the magnetization curve is considered accurately. Thus, the magnetization curve illustrated in Figure 3(c) is used for the current transformer core. This single-valued magnetization curve is used for the current transformer. Since the hysteresis characteristic does not considerably affect the current transformer transient behavior [27], the single-valued curve is an appropriate curve for transient analysis of the current transformer and can be used instead of a multi-valued curve. According to Figure 3(c):

$$i_\mu = \begin{cases} \frac{\psi_\mu - \psi_s}{L_s} + i_{\mu_0} & \psi_\mu > \psi_s \\ \frac{\psi_\mu + \psi_s}{L_s} - i_{\mu_0} & \psi_\mu < -\psi_s \\ i_{\mu_0}\frac{\psi_\mu}{\psi_s} & |\psi_\mu| \leq \psi_s \end{cases} \tag{30}$$

In this equation, ψ_μ represents the flux linkages, ψ_s represents the flux linkages at the saturation knee point of the magnetization curve, i_{μ_0} represents the magnetization current at the saturation knee point of the magnetization curve, and L_s represents the slope of the saturation zone. To model the current transformer, the equivalent circuit shown in Figure 3(b) is considered. In this circuit, we defined:

$$R = R_2 + R_b, \qquad L = L_2 + L_b. \tag{31}$$

According to the equivalent circuit shown in Figure 3(b):

$$i_{ps} = i_\mu + i_s, \tag{32}$$

$$e_s = Ri_s + L\frac{di_s}{dt}, \tag{33}$$

$$i_{ps} = \frac{N_p}{N_s} i_p. \tag{34}$$

In these equations, i_{ps} represents the primary current that refers to the secondary side, i_μ is the magnetizing current, i_s is the secondary current, N_p is the number of primary turns, N_s is the number of secondary turns, and e_s represents the induced voltage in the secondary winding. According to Eq. (32):

$$i_s = i_{ps} - i_\mu. \tag{35}$$

According to Figure 3(c), the magnetization curve of the current transformer has three regions.

For region 1, $\psi_\mu > \psi_s$:

$$i_\mu = \frac{(\psi_\mu - \psi_s)}{L_s} + i_{\mu_0}. \tag{36}$$

According to Eqs. (35) and (36):

$$i_s = i_{ps} - \frac{1}{L_s}(\psi_\mu - \psi_s) - i_{\mu_0}. \tag{37}$$

Differentiate from Eq. (37):

$$\frac{di_s}{dt} = \frac{di_{ps}}{dt} - \frac{1}{L_s}\frac{d\psi_\mu}{dt}. \tag{38}$$

Due to $\frac{d\psi_\mu}{dt} = e_s$, from Eqs. (33), (37) and (38):

$$\begin{aligned}\frac{d\psi_\mu}{dt} =& \frac{RL_s}{L_s+L}\left(i_{ps} - \frac{(\psi_\mu - \psi_s)}{L_s} - i_{\mu_0}\right)\\ &+ \frac{LL_s}{L_s+L}\left(\frac{di_{ps}}{dt}\right).\end{aligned} \tag{39}$$

For region 2, $\psi_\mu < -\psi_S$:

$$i_\mu = \frac{1}{L_s}(\psi_\mu + \psi_s) - i_{\mu_0}. \tag{40}$$

According to Eqs. (35) and (40):

$$i_s = i_{ps} - \frac{1}{L_s}(\psi_\mu + \psi_s) + i_{\mu_0}. \tag{41}$$

Differentiate from Eq. (41):

$$\frac{di_s}{dt} = \frac{di_{ps}}{dt} - \frac{1}{L_s}\frac{d\psi_\mu}{dt}. \tag{42}$$

Due to $\frac{d\psi_\mu}{dt} = e_s$, from Eqs. (33), (41) and (42):

$$\begin{aligned}\frac{d\psi_\mu}{dt} =& \frac{RL_s}{L_s+L}\left(i_{ps} - \frac{(\psi_\mu + \psi_s)}{L_s} + i_{\mu_0}\right)\\ &+ \frac{LL_s}{L_s+L}\left(\frac{di_{ps}}{dt}\right).\end{aligned} \tag{43}$$

For region 3, $|\psi_\mu| \leq \psi_s$:

$$i_\mu = i_{\mu_0}\frac{\psi_\mu}{\psi_s}. \tag{44}$$

According to Eqs. (35) and (44):

$$i_s = i_{ps} - i_{\mu_0}\frac{\psi_\mu}{\psi_s}. \tag{45}$$

Differentiate from Eq. (45):

$$\frac{di_s}{dt} = \frac{di_{ps}}{dt} - \frac{i_{\mu_0}}{\psi_s}\frac{d\psi_\mu}{dt}. \tag{46}$$

Due to $\frac{d\psi_\mu}{dt} = e_s$, from Eqs. (33), (45) and (46):

$$\frac{d\psi_\mu}{dt} = \frac{R\psi_s}{\psi_s + Li_{\mu_0}}\left(i_{ps} - i_{\mu_0}\frac{\psi_\mu}{\psi_s}\right) + \frac{L\psi_s}{\psi_s + Li_{\mu_0}}\left(\frac{di_{ps}}{dt}\right). \tag{47}$$

3. Proposed algorithm for the differential protection

The differential protection should be able to distinguish between internal and external faults, the magnetizing inrush current and the ultra-saturation phenomenon, and it should only operate under internal faults. Several studies have been done to distinguish internal faults from external faults and magnetic inrush current by various algorithms, but, in all studies, the ultra-saturation phenomenon was not taken into account. In this paper, at first, a new model for investigating the ultra-saturation phenomenon during the energization of a loaded three-phase power transformer is presented. For modeling the ultra-saturation phenomenon, modeling of the power transformer and the current transformer on the primary and secondary sides of the power transformer is required. So, by using Eqs. (1)-(29), the power transformer is modeled, as described in Section 2.1. By using Eqs. (1)-(29), the magnetic linkage of the transformer core and the primary and secondary currents of the three-phase power transformer are calculated. The primary currents of the power transformer are the primary currents of the current transformers on the primary side of the power transformer, and the secondary currents of the power transformer are the primary currents of the current transformers on the secondary side of the power transformer. The differential currents are calculated by subtraction between secondary currents of the current transformers on the primary and secondary sides of the power transformer, and they will reach the differential relay. Therefore, to calculate the differential currents, modeling of the current transformer is required using Eqs. (30)-(47) in Section 2.2. On the other hand, using Eqs. (1)-(47) for the power transformer and the current transformers, the ultra-saturation phenomenon is modeled and the unusually false trip of the differential protection due to the ultra-saturation phenomenon is presented using the DFT algorithm of the differential currents. In this algorithm, the PSACAD program is also used for simulating the inrush current, and internal and external faults. Normally, in order to distinguish between external faults, internal faults and magnetizing inrush current, an algorithm is used in which the differential protection operates when the amplitude of the basic component of the differential current fixes higher than 0.25 p.u, and the level of the second harmonic to the basic harmonic of the differential current fixes lower than 15%. However, it has been shown that under certain conditions, the false trip of the differential protection under the ultra-saturation phenomenon has lead to the tripping of healthy transformers. In this algorithm, to distinguish internal from external faults, the magnetizing inrush current and the ultra-saturation phenomenon, first the differential currents of phases are obtained from subtraction of the secondary currents of the current transformers from the primary and secondary sides of the power transformers. Then, to distinguish between transient phenomena, appropriate criteria using signal harmonic components of differential currents will be presented by the DFT algorithm. Finally, the following steps are performed to distinguish transient phenomena:

a) At first, the ratio of the second harmonic to the basic harmonic ($\frac{H_2}{H_{\text{base}}}$) of the differential currents is calculated by the use of the DFT algorithm. If the ratio fixes higher than 15%, the inrush current will occur. Otherwise, the other transient phenomena may occur.
b) In the next step, the steady state amplitudes of the basic component of the differential currents (i_{dss}) are calculated using the DFT algorithm. If the steady state amplitudes fix lower than 0.25 p.u., external faults will occur. Otherwise, the ultra-saturation phenomenon or internal faults may occur.
c) In the last step, to distinguish between the ultra-saturation phenomenon and the internal faults, the ratio of the seventh harmonic to the fifth harmonic ($\frac{H_7}{H_5}$) of the differential currents is calculated using the DFT algorithm. If this ratio stabilizes below 20%, an internal fault occurs and the differential protection must operate.

On the other hand, if the amplitudes of the differential currents stabilize higher than 0.25 p.u., the ratio change of the second harmonic to the basic harmonic stabilizes lower than 15% and the seventh harmonic to the fifth harmonic stabilizes lower than 20%, an internal fault occurs and a differential relay should be operated. Otherwise, the other transient phenomena may occur and the differential relay will not operate. To prove the results in the next section, the proposed algorithm is investigated for various cases of transient phenomena. The flowchart of the proposed algorithm is shown in Figure 4.

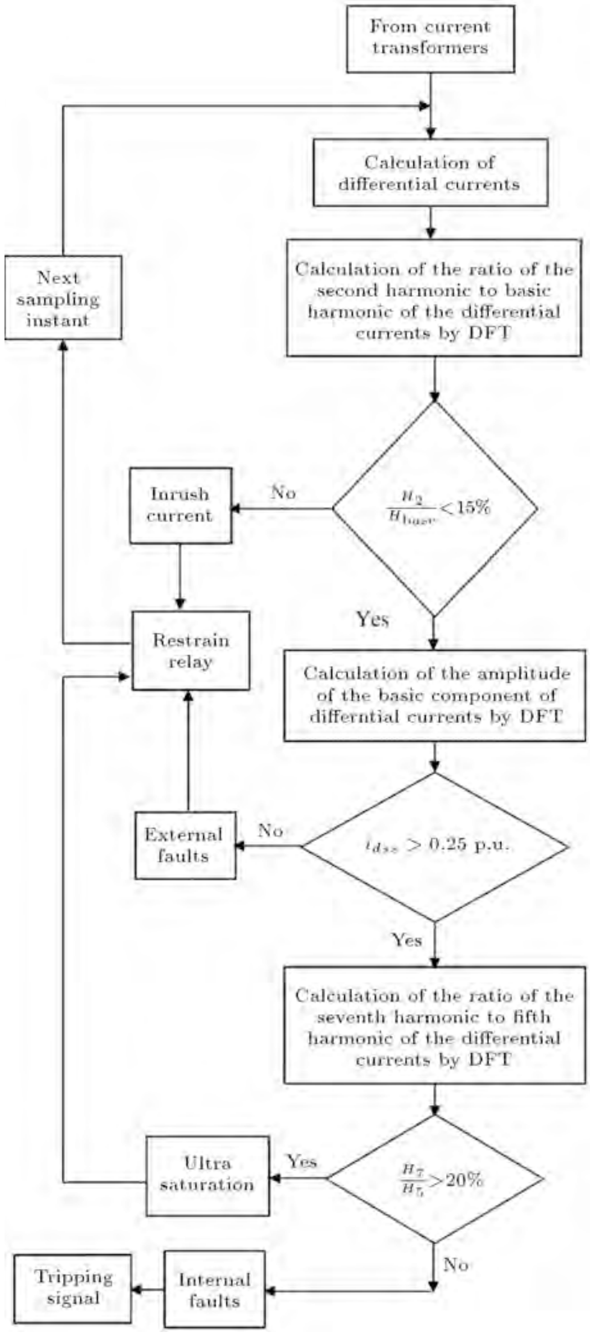

Figure 4. The flowchart of the proposed algorithm.

4. Simulation results

4.1. Simulation of the ultra-saturation phenomenon

It is supposed that the three-phase power transformer is load connected and is switched on from the high-voltage side at $t = 0$. The source and three-phase power transformer parameters are:

$$u_{pa} = U_m \sin(\omega t + \theta),$$

$$u_{pb} = U_m \sin(\omega t + \theta - 120°),$$

$$u_{pc} = U_m \sin(\omega t + \theta - 240°),$$

$$U_m = 400 \text{ kV}, \qquad \omega = 100\pi \text{ rad}, \qquad \theta = 80°,$$

$$k = 400/230 \text{ kV}, \qquad R_p = 0.9\ \Omega,$$

$$L_{dp} = 0.1019 \text{ H}, \qquad R_s = 0.5\ \Omega,$$

$$L_{ds} = 0.0337 \text{ H}, \qquad N_p = 610,$$

$$N_s = 352, \qquad R_b = 5\ \Omega, \qquad L_b = 0.3029 \text{ H},$$

$S = 500$ MVA, $\Re_d = 2500$ A.t/Wb,

$f_{0a} = 10.05$ A.t, $p_a = 5$,

$k_{1a} = 28$ Wb/A.t, $k_{2a} = 0.995$ Wb/A.t,

$f_{0b} = 10.03$ A.t, $p_b = 5$,

$k_{1b} = 45$ Wb/A.t, $k_{2a} = 0.9152$ Wb/A.t,

$f_{0c} = 10.05$ A.t, $p_c = 5$,

$k_{1c} = 28$ Wb/A.t, $k_{2c} = 0.9134$ Wb/A.t.

$\phi_a(0) = 1.5878\ \mathrm{e}^{-3}$wb, $\phi_b(0) = 4.7619\ \mathrm{e}^{-3}$ wb,

$\phi_a(0) = -6.3518\ \mathrm{e}^{-3}$wb.

Parameters for the current transformer on the high-voltage side of the power transformer are:

$k = 600/5$, $B_s = 1.8$ T, $L_s = 0.7$ mH,

$A = 3.472\ \mathrm{e}^{-3}\mathrm{m}^2$, $\psi_s = 0.75$ (wb*turns),

$i_{\mu_0} = 0.05$ mA, $R = 0.05\ \Omega$.

Parameters for the current transformer on the low-voltage side of the power transformer are:

$k = 1000/5$, $B_s = 1.9$ T, $L_s = 0.7$ mH,

$A = 3.53\ \mathrm{e}^{-3}\mathrm{m}^2$, $\psi_s = 1.34$ (wb*turns),

$i_{\mu 0} = 0.03$ mA, $R = 0.15\ \Omega$.

For modeling of the ultra-saturation phenomenon, i_{pa}, i_{pb}, i_{pc}, i_a, i_b, i_c, ϕ_a, ϕ_b and ϕ_c can be solved from Eqs. (1)-(4), (11), (16) and (23)-(29). i_{pa}, i_{pb}, i_{pc}, i_a, i_b and i_c are the primary and secondary currents of the three-phase power transformer. i_{pa}, i_{pb} and i_{pc} are the primary currents of current transformers on the primary side of the power transformer, and i_a, i_b and i_c are the primary currents of current transformers on the secondary side of the power transformer. Now, the secondary currents of the current transformers on the primary and secondary sides of the power transformer should be calculated. ψ_μ is related to the current transformers on the primary and secondary sides of the power transformer, and can be solved from Eqs. (39), (43) and (47) using the fourth-order Runge-Kutta method with a 10μs time step. The magnetic current, i_μ, according to Eq. (30), and the secondary current of the current transformers, according to given Eqs. (37), (41) and (45), have been calculated using the computed ψ_μ. In these relations, i_{ps} is the primary current of the power transformer. The wave forms of the magnetic linkage of the transformer core, and the primary and secondary currents of the three-phase power transformer due to ultra-saturation are shown in Figures 5(a), 5(b) and 5(c), respectively. The differential currents (i_d) due to the ultra-saturation phenomenon that are calculated by subtraction between the secondary currents of the current transformers on the primary and secondary sides of the power transformer is shown in Figure 5(d). Figure 6(a) displays the changes of the amplitudes of the basic component of the differential currents in Figure 5(d), obtained with the DFT algorithm. In this figure, the amplitudes of the basic component of

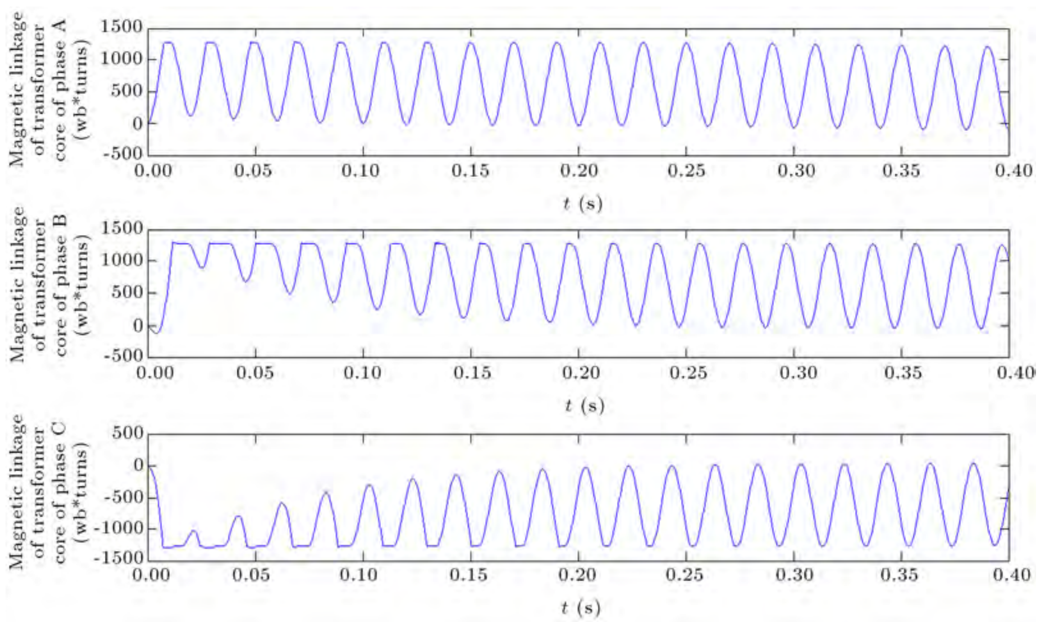

Figure 5a. Wave shapes of the magnetic linkage of transformer core due to the ultra-saturation phenomenon.

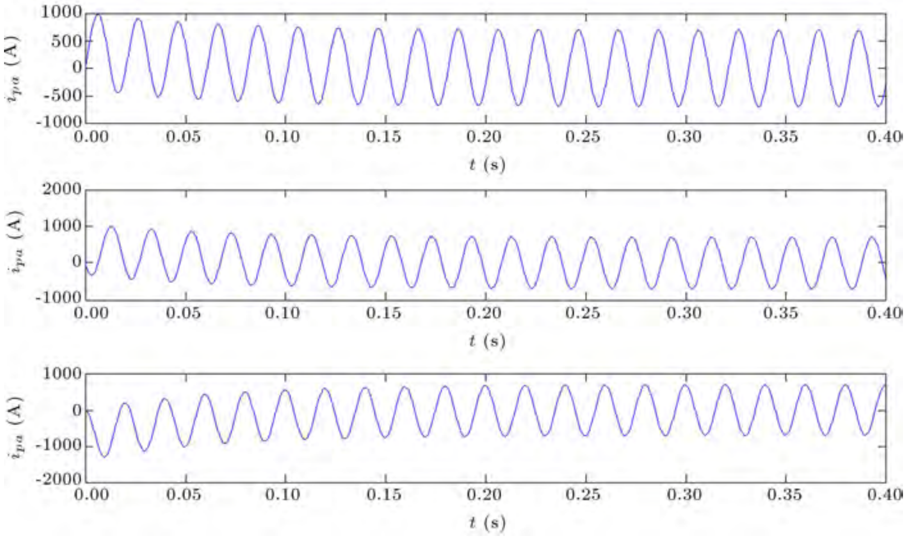

Figure 5b. Wave shapes of the primary currents of transformer due to the ultra-saturation phenomenon.

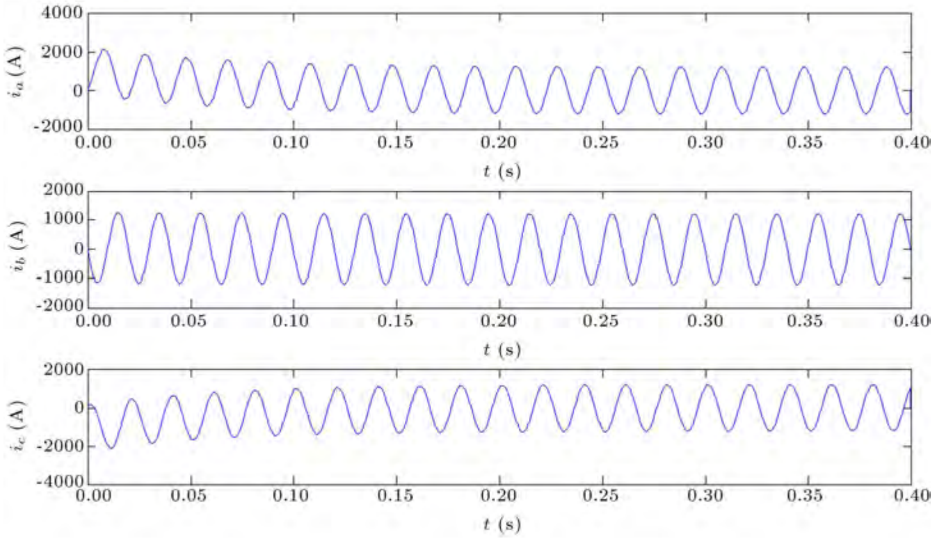

Figure 5c. Wave shapes of the secondary currents of transformer due to the ultra-saturation phenomenon.

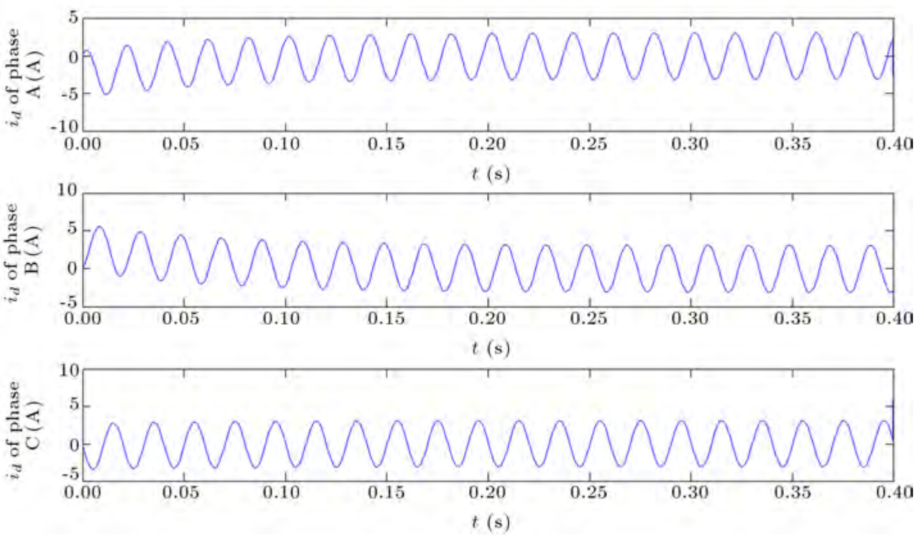

Figure 5d. Wave shapes of differential currents due to the ultra-saturation phenomenon.

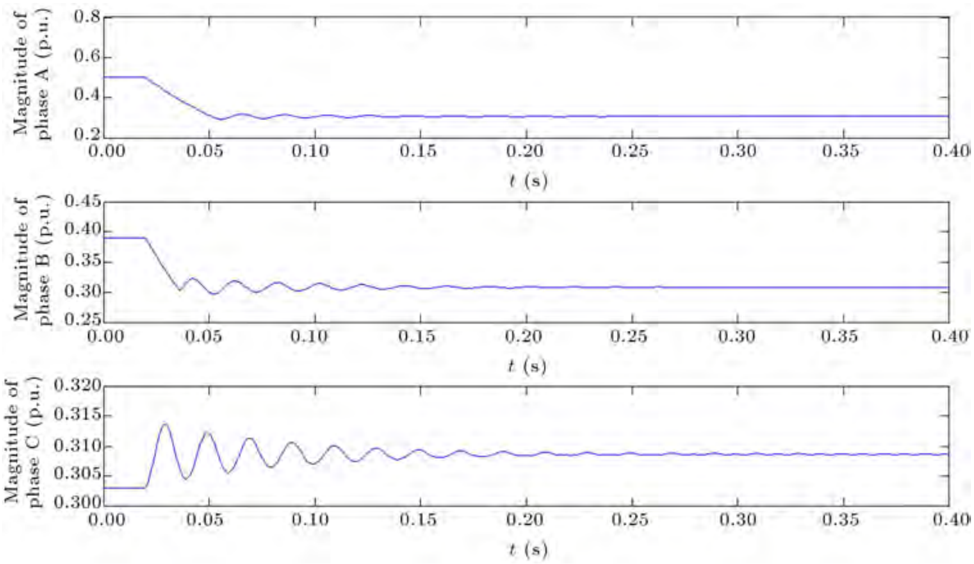

Figure 6a. The normalized amplitudes of the basic component of the differential currents with DFT algorithm due to the ultra-saturation phenomenon.

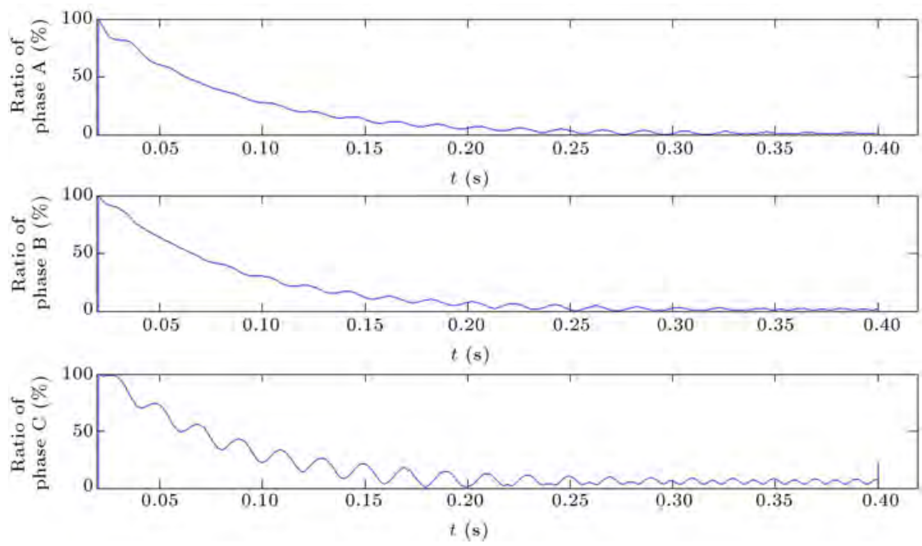

Figure 6b. The ratio of the second harmonic to basic harmonic of the differential currents with DFT algorithm due to the ultra-saturation phenomenon.

the differential current are normalized according to the secondary current of the current transformers (5A). Figure 6(b) displays the ratio change of the second harmonic to the basic harmonic of the differential currents, which is obtained with the DFT algorithm. As illustrated in Figure 6(a), the basic component of the differential currents is above 0.25 p.u. From the beginning of energization and after, approximately, 6 cycles, it is stabilized above 0.25 p.u. Also, according to Figure 6(b), as the energization time exceeds 0.1344 s, 0.1463 s and 0.1537 s for A, B, and C phases, respectively, the ratio of the second harmonic to the basic harmonic stabilizes lower than 15%. So, according to Figures 6(a) and 6(b), if the differential protection uses 0.25 p.u. as the operating threshold for the amplitudes of the basic component of differential currents, and 15% as the second harmonic restraint ratio, the false trip occurs at 0.1344s.

4.2. Simulation of the inrush current

If the amplitude and polarity of the residual flux are not in agreement with the amplitude and polarity of the instantaneous value of the steady state flux, inrush current happens. So, when a transformer is switched on, inrush currents are caused by saturation effects in the magnetic core. One of the important characteristics of inrush current in the differential relay is the second harmonic. The level of the second harmonic in inrush current is high, and the value of the second harmonic is a function of the degree of saturation. Hence, to

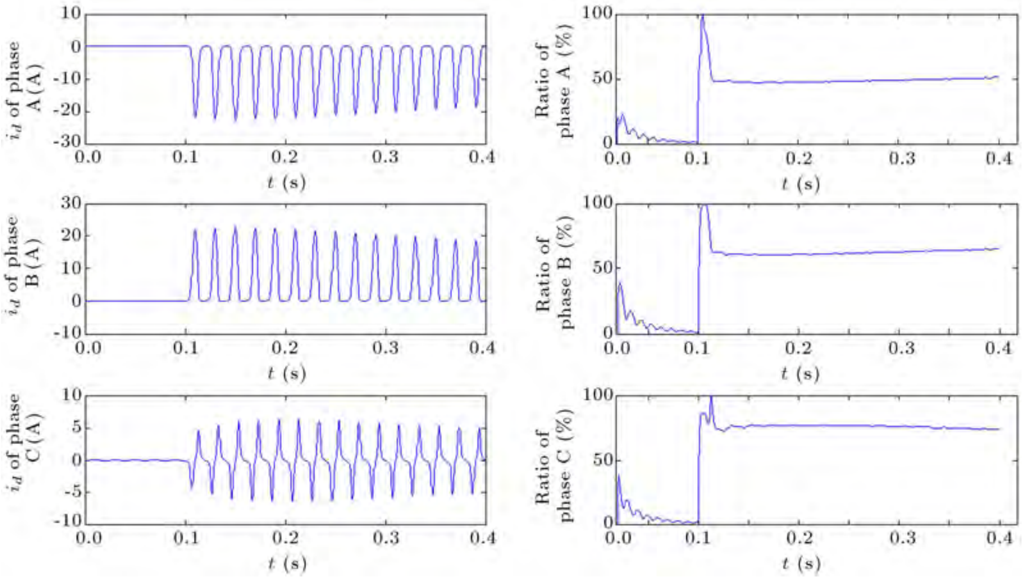

Figure 7a. The differential currents and the ratio of the second harmonic to basic harmonic of the differential currents due to inrush current by the change of the residual flux.

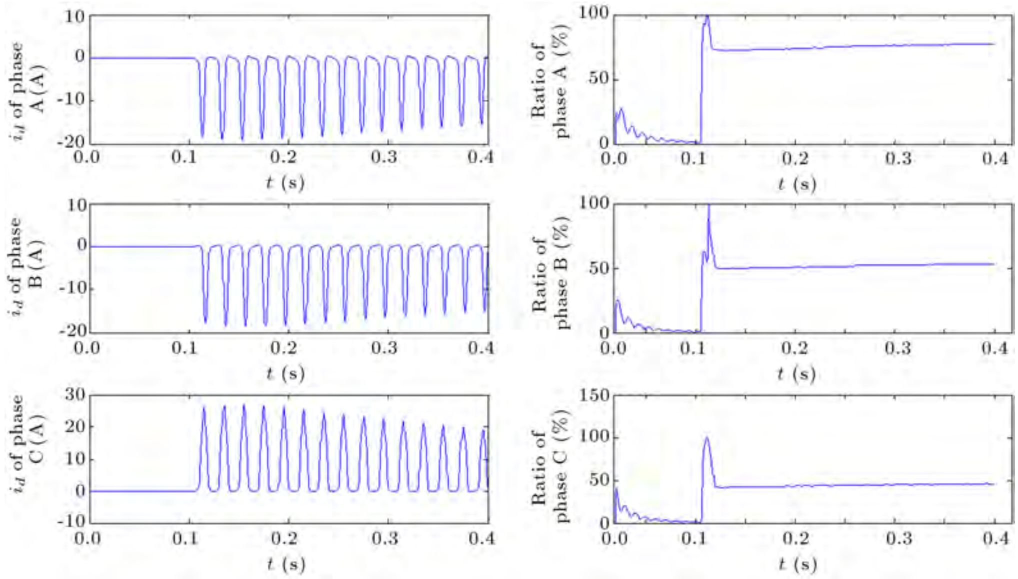

Figure 7b. The differential currents and the ratio of the second harmonic to basic harmonic of the differential currents due to inrush current by the change of the switching time.

determine the degree of saturation caused by transient inrush currents from steady state currents, the content of the second harmonic is used. So, in the proposed algorithm, the second harmonic is used for distinguishing inrush current from steady state currents and other transient phenomena. For simulation of the inrush current, the unloading transformer is switched on at 0.1 s. Showing the accuracy of the proposed algorithm under all conditions, various test signals by changing some parameters are simulated. Some important parameters such as residual flux, switching time and inception angle have a direct impact on magnetic inrush currents. So, to prove the results of the proposed algorithm, some different signals due to inrush current are generated by the change of residual flux, switching time and inception angle. At various transient inrush currents in the power transformer, 60 test signals for different condition of the inrush current are simulated. Due to limitation of paper length, some cases of inrush current are shown in Figures 7(a), 7(b) and 7(c). In these figures, the differential currents and the ratio of the second harmonic to the basic harmonic of the differential currents due to inrush current, by changes in residual flux, switching time and inception angle, are shown. According to these figures, the ratio change of the second harmonic to the basic harmonic of the

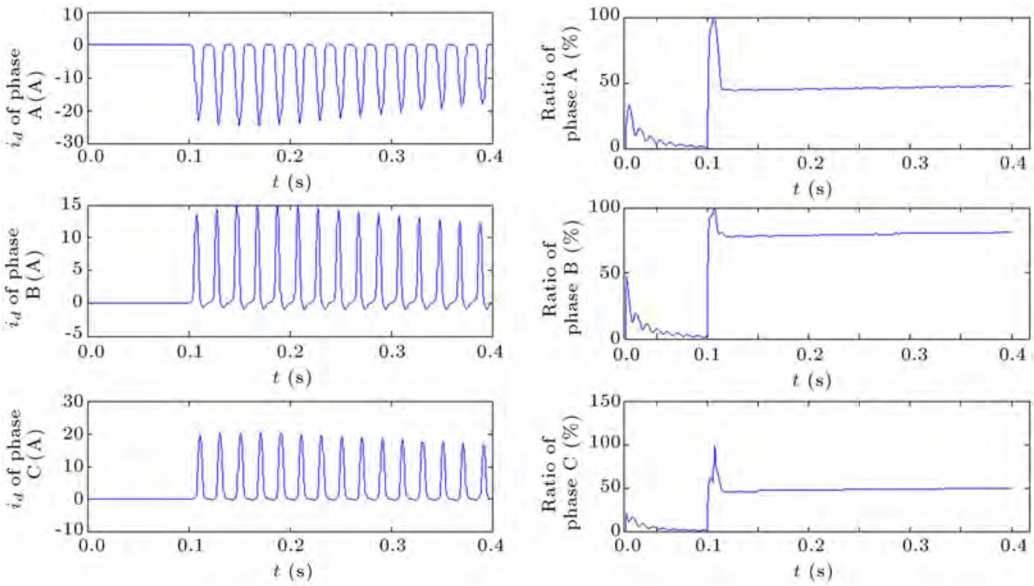

Figure 7c. The differential currents and the ratio of the second harmonic to basic harmonic of the differential currents due to inrush current by the change of the inception angle.

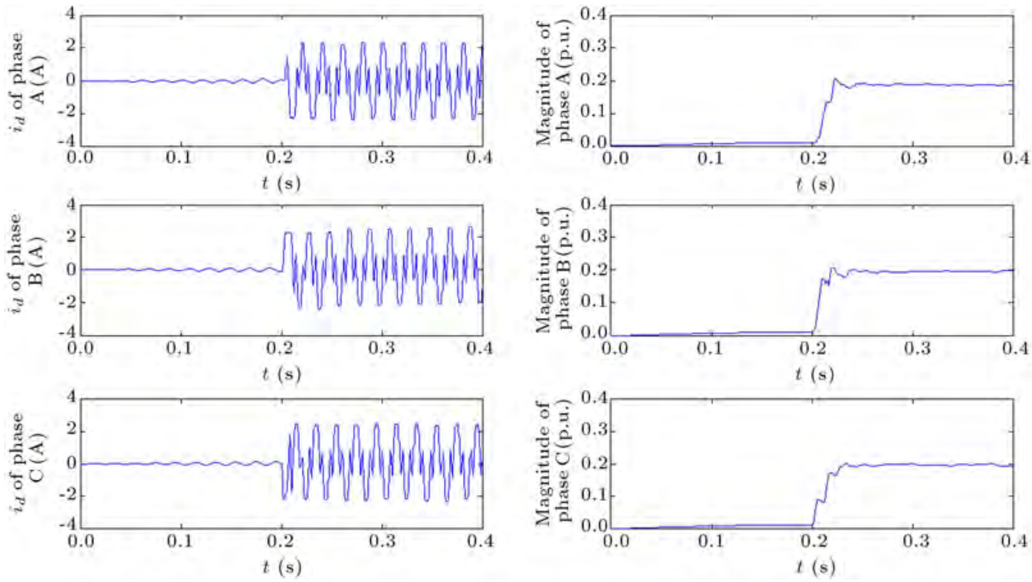

Figure 8a. The differential currents and the normalized amplitudes of the basic component of the differential currents due to the three-phase external fault by the change of the residual flux.

differential currents due to the inrush current always stabilizes higher than 15%. Therefore, the differential protection under the inrush current condition will not operate. The obtained results for inrush current show the accuracy of the proposed algorithm.

4.3. Simulation of the external faults

For simulation of the external faults, PSCAD and MATLAB programs are used. Fault is occurred on the outside of the protective zone of the differential relay on the load side. The simulated fault types are the three-phase fault, the three-phase-to-ground fault, the phase-to-ground fault, the phase-to-phase fault and the phase-to-phase-to-ground fault. In the external faults, different signals are generated by the change of the residual flux, load level, fault resistance, inception angle and fault occurrence time. At various transient external faults in the power transformer, 500 test signals for different conditions of external faults are simulated. Due to the limitation of paper length, some cases of external faults by changes in residual flux, load level, fault resistance, inception angle and fault occurrence time are shown in Figures 8(a) to 8(e). For simulation of the external faults, the time of fault occurrence is considered 0.2 s. In these figures, the differential currents and the steady state ampli-

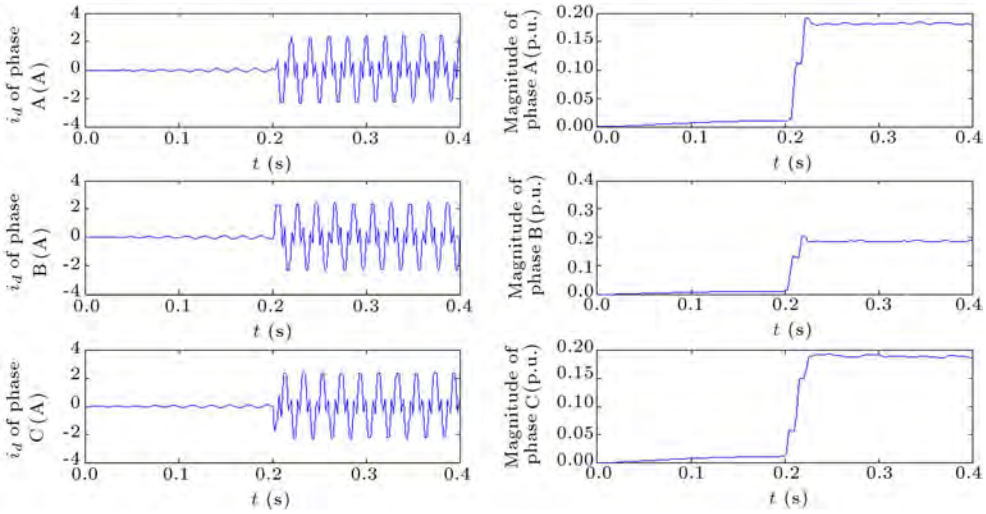

Figure 8b. The differential currents and the normalized amplitudes of the basic component of the differential currents due to the three-phase-to-ground external fault by the change of the load level.

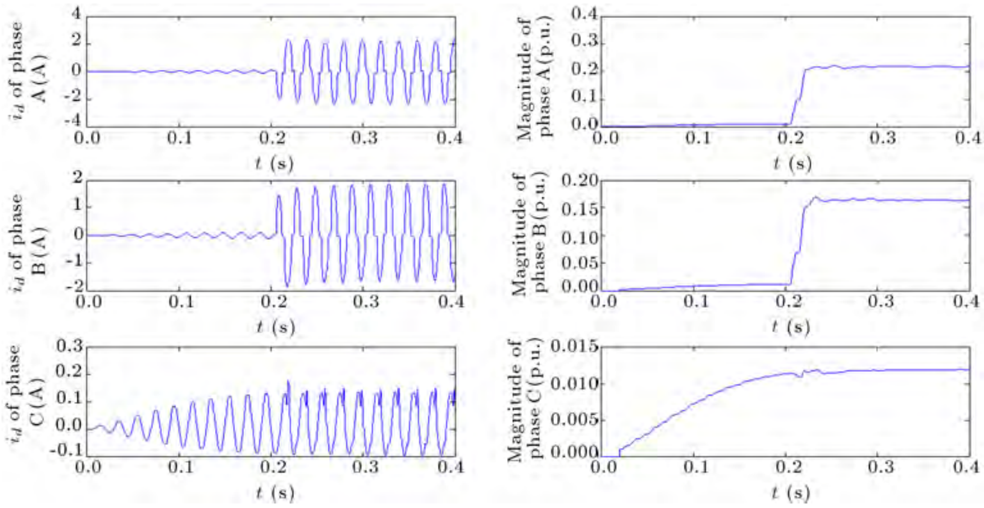

Figure 8c. The differential currents and the normalized amplitudes of the basic component of the differential currents due to the phase-to-phase external fault by the change of the occurrence time.

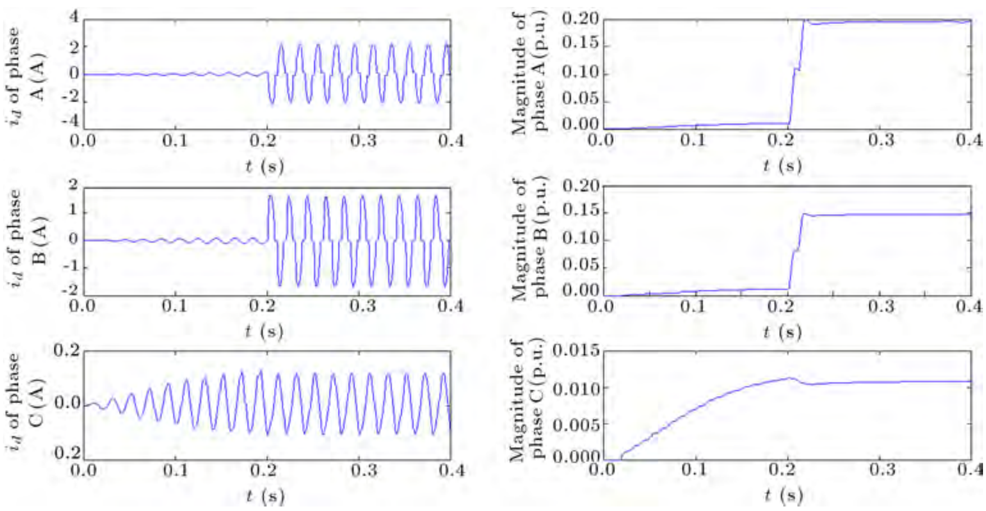

Figure 8d. The differential currents and the normalized amplitudes of the basic component of the differential currents due to the phase-to-phase-to-ground external fault by the change of the inception angle.

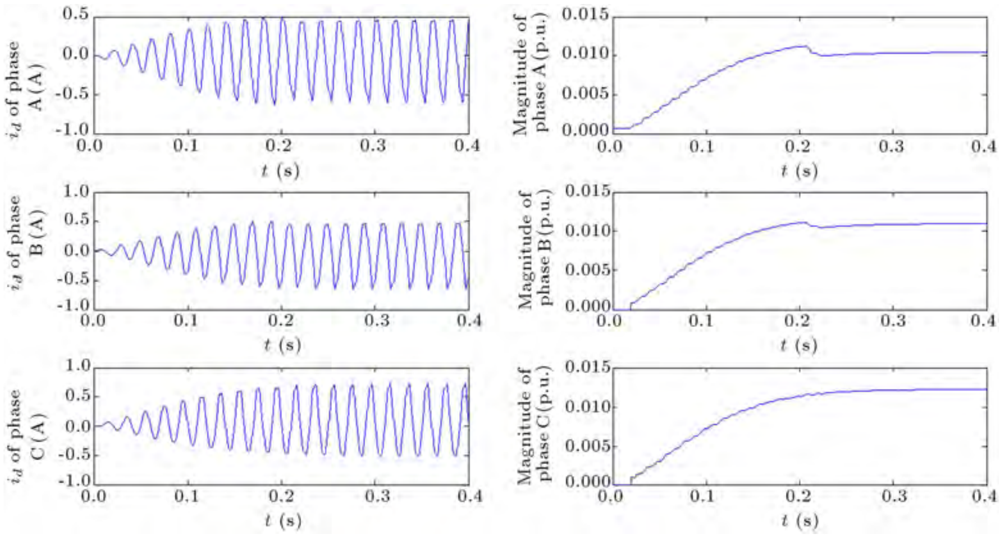

Figure 8e. The differential currents and the normalized amplitudes of the basic component of the differential currents due to the phase-to-ground external fault by the change of the fault resistance.

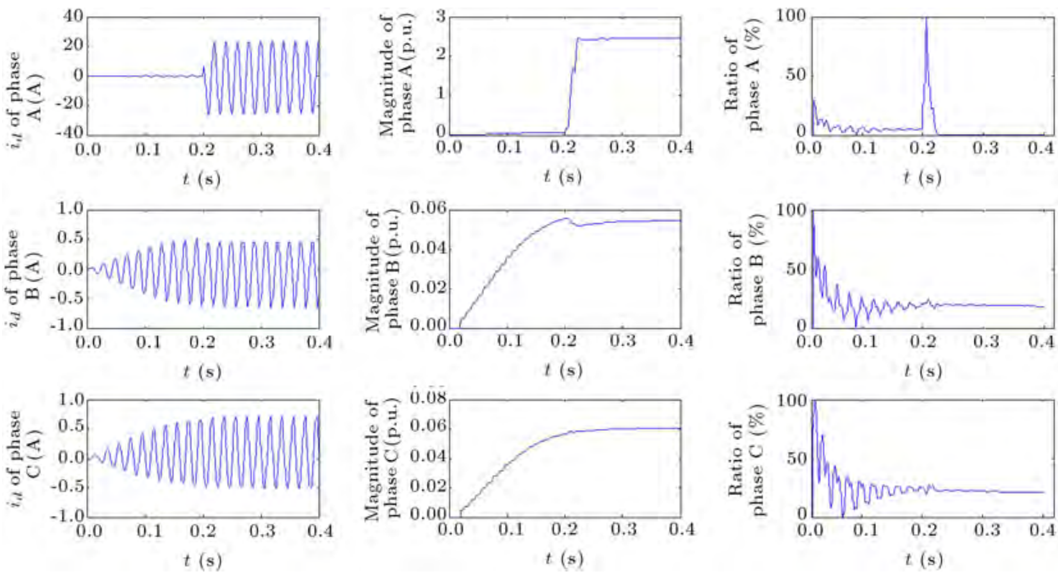

Figure 9a. The differential currents, the normalized amplitudes of the basic component of the differential currents and the ratio of the second harmonic to basic harmonic of the differential currents due to the turn-to-ground internal fault by the change of the residual flux.

tudes of the differential currents due to the external faults by changes in residual flux, load level, fault resistance, inception angle and fault occurrence time are shown. According to these figures, the amplitudes of the differential currents due to the external faults stabilize lower than 0.25 p.u. Therefore, the differential protection under the external faults condition will not operate.

4.4. Simulation of the internal faults

For simulating the internal faults of the power transformer which involve turn-to-ground, turn-to-turn and phase-to-phase, PSCAD and MATLAB programs are also used. In the turn-to-ground fault, the fault is occurred on the secondary winding of phase A at the 25% position of winding, and in the turn-to-turn fault, the fault is occurred on the secondary winding of phase A in which 10 percent of the turns are short circuited. In the phase-to-phase fault, the fault is occurred on the secondary windings of phases A and B at the 25% position of windings. In the internal faults, different signals are generated by the changes in residual flux, load level, fault resistance, inception angle and fault occurrence time. At various transient internal faults in the power transformer, 300 test signals for different conditions of internal faults are simulated. Due to the limitation of paper length, some cases of internal faults are shown in Figures 9(a), 9(b) and 9(c). For simu-

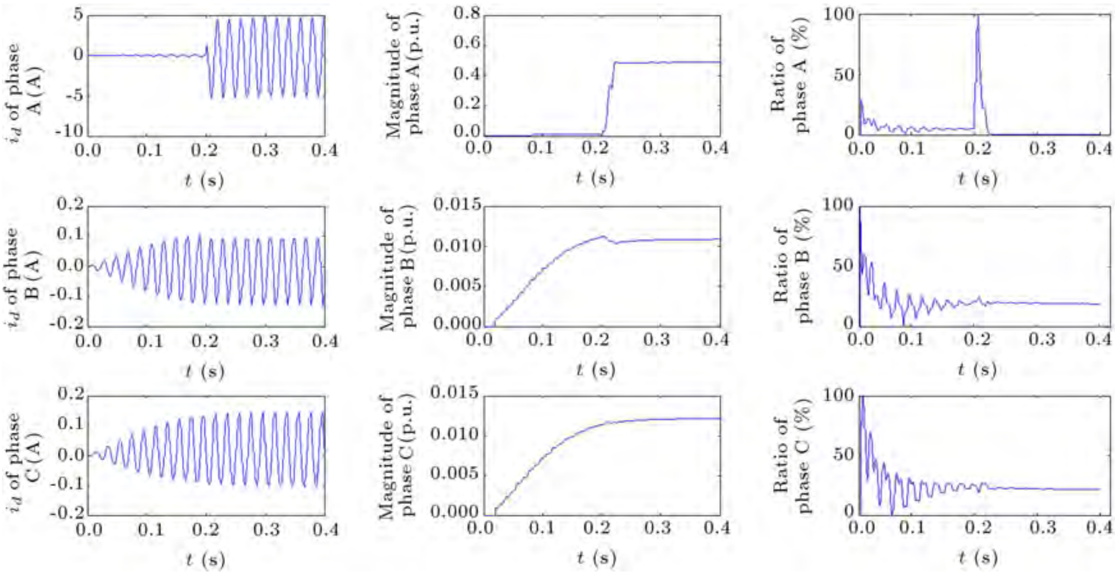

Figure 9b. The differential currents, the normalized amplitudes of the basic component of the differential currents and the ratio of the second harmonic to basic harmonic of the differential currents due to the turn-to-turn internal fault by the change of the load level.

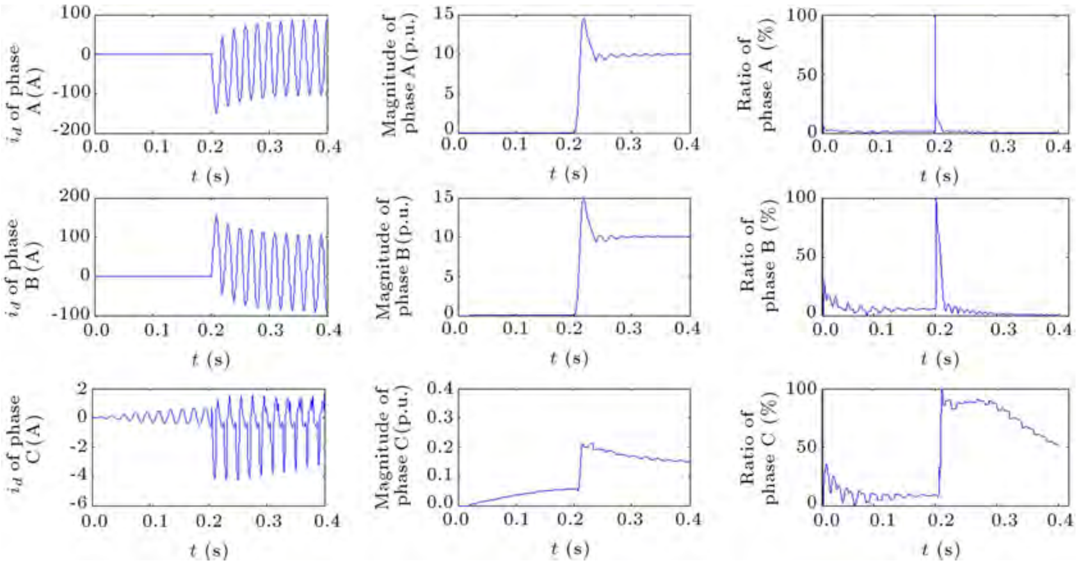

Figure 9c. The differential currents, the normalized amplitudes of the basic component of the differential currents and the ratio of the second harmonic to basic harmonic of the differential currents due to the phase-to-phase internal fault by the change of the inception angle.

lation of internal faults, the time of fault occurrence is considered 0.2 s. In these figures, the differential currents, the steady state amplitudes of the differential currents and the ratio of the second harmonic to basic harmonic of the differential currents, due to internal faults, by changes in residual flux, load level and inception angle, are shown. According to these figures, the amplitudes of the basic component and the ratio change of the second harmonic to the basic harmonic of the differential currents, due to internal faults, exceed threshold values and the differential protection will operate.

4.5. Distinguish between the ultra-saturation phenomenon and the internal faults

According to simulations, if the differential protection uses 0.25 p.u. as the operating threshold for amplitudes of differential currents, and 15% as the second harmonic restraint ratio, the differential relay, due to the ultra-saturation phenomenon and the internal faults, will operate. The differential relay is used for protecting transformers against internal faults, but it should not operate under the ultra-saturation phenomenon. Therefore, to distinguish the internal faults from the ultra-saturation phenomenon,

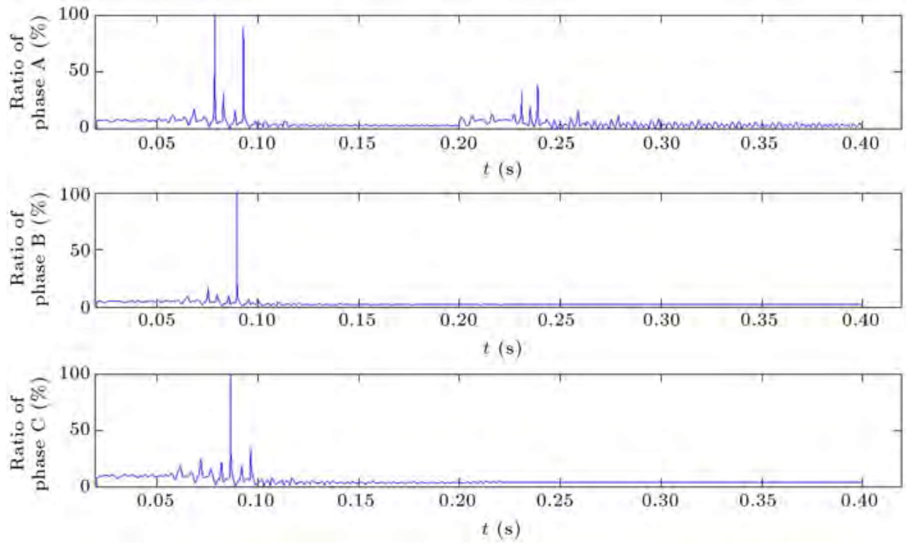

Figure 10a. The ratio of the seventh harmonic to the fifth harmonic of the differential currents due to the turn-to-ground internal fault by the change of the residual flux.

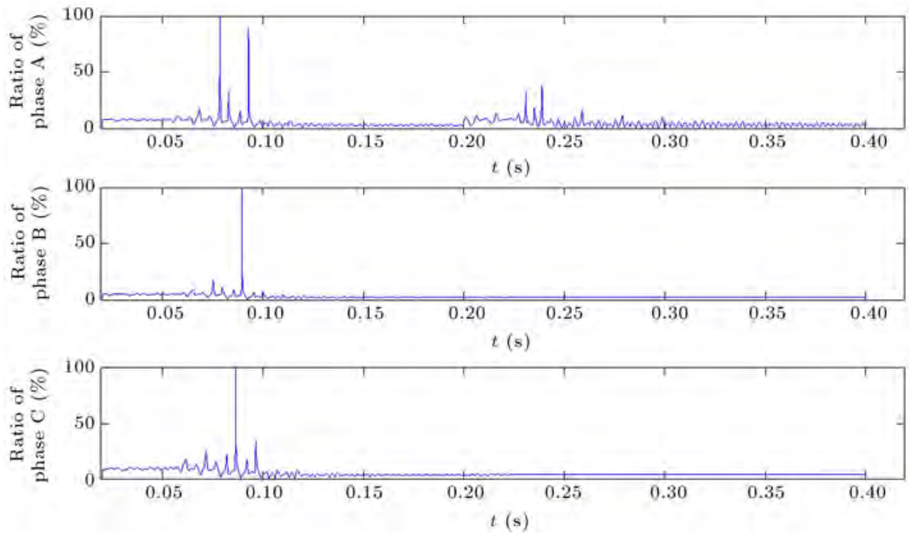

Figure 10b. The ratio of the seventh harmonic to the fifth harmonic of the differential currents due to the turn-to-turn internal fault by the change of the load level.

the ratio of the seventh harmonic to the fifth harmonic is another criterion that is necessary for preventing the false trip of the differential protection due to the ultra-saturation phenomenon. At various transient phenomena in the power transformer, 380 test signals involving internal faults and the ultra-saturation phenomenon are simulated. In the ultra-saturation phenomenon, different signals are generated by the changes in residual flux, load level, inception angle and different state of current transformer saturation. In the internal faults, as mentioned, different signals are generated by the changes in residual flux, load level, fault resistance, inception angle and fault occurrence time. Figures 10(a), 10(b) and 10(c) show the ratio change of the seventh harmonic to the fifth harmonic of the differential currents, due to internal faults, and Figures 11(a) to 11(d) show the differential currents and the ratio change of the seventh harmonic to the fifth harmonic of the differential currents, due to the ultra-saturation phenomenon, which are obtained with the DFT algorithm. According to these figures, if the ratio change of the seventh harmonic to the fifth harmonic of the differential currents stabilizes lower than 20%, an internal fault occurs and the differential protection should operate. On the other hand, if the amplitudes of the differential currents stabilize higher than 0.25 p.u., the ratio change of the second harmonic to the basic harmonic stabilizes lower than 15% and the seventh harmonic to the fifth harmonic stabilizes higher than 20%, the ultra-saturation phenomenon occurs and the differential relay, due to the ultra-saturation phenomenon, will not operate. As mentioned, this

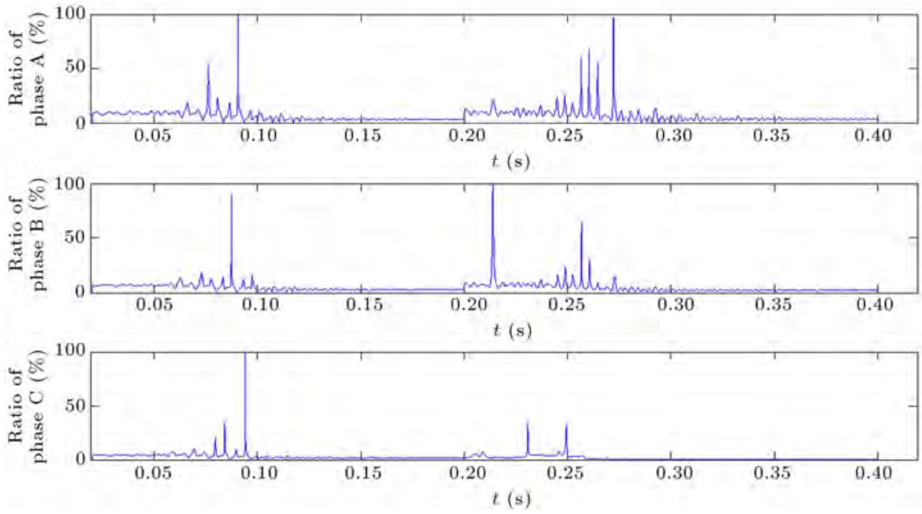

Figure 10c. The ratio of the seventh harmonic to the fifth harmonic of the differential currents due to the phase-to-phase internal fault by the change of the inception angle.

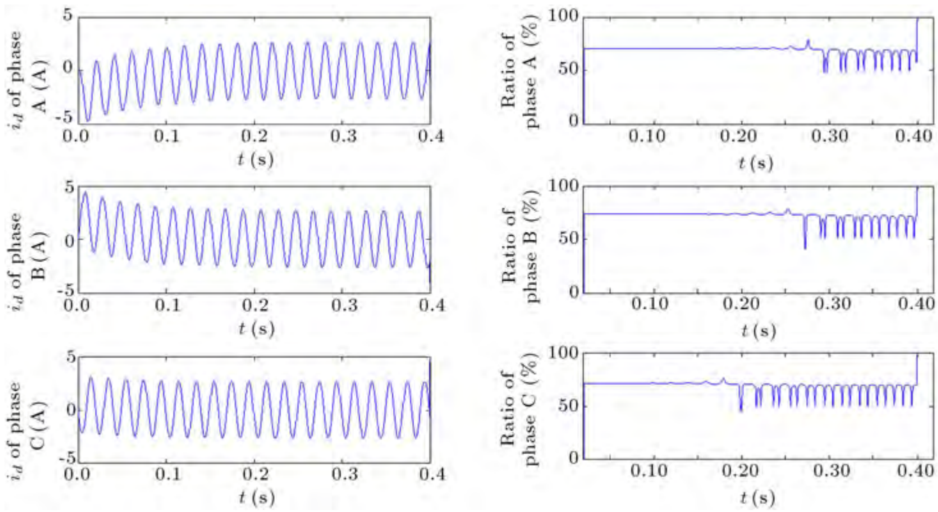

Figure 11a. The differential currents and the ratio of the seventh harmonic to the fifth harmonic of the differential currents due to the ultra-saturation phenomenon by the change of the residual flux.

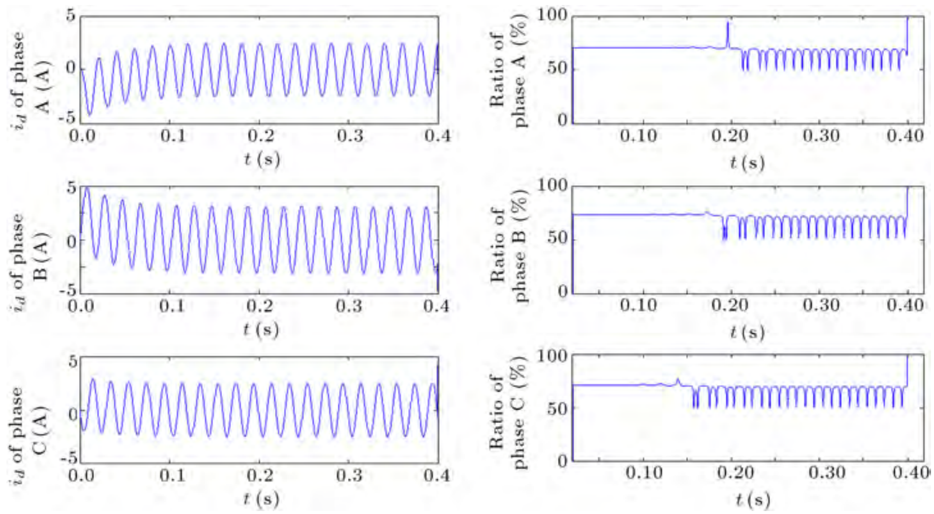

Figure 11b. The differential currents and the ratio of the seventh harmonic to the fifth harmonic of the differential currents due to the ultra-saturation phenomenon by the change of the load level.

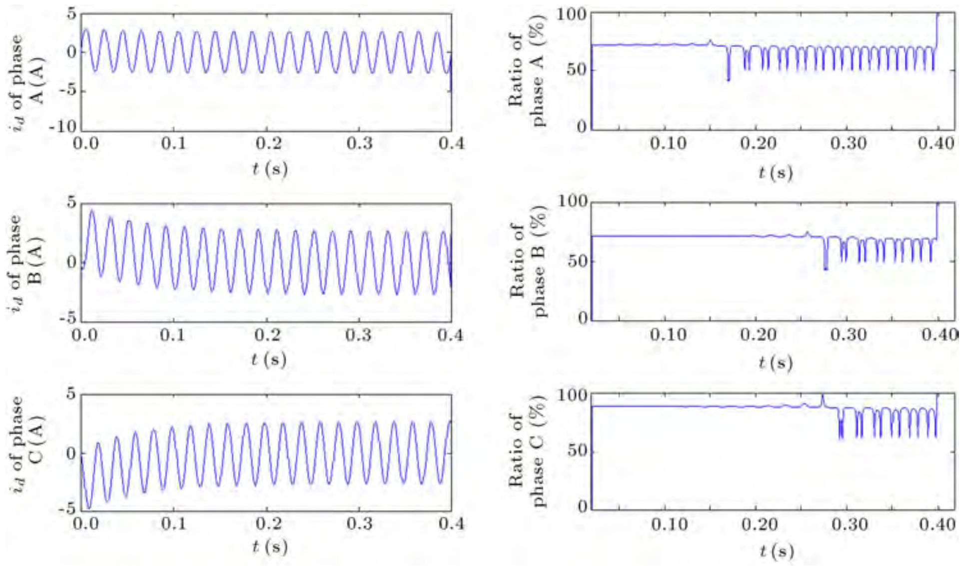

Figure 11c. The differential currents and the ratio of the seventh harmonic to the fifth harmonic of the differential currents due to the ultra-saturation phenomenon by the change of the inception angle.

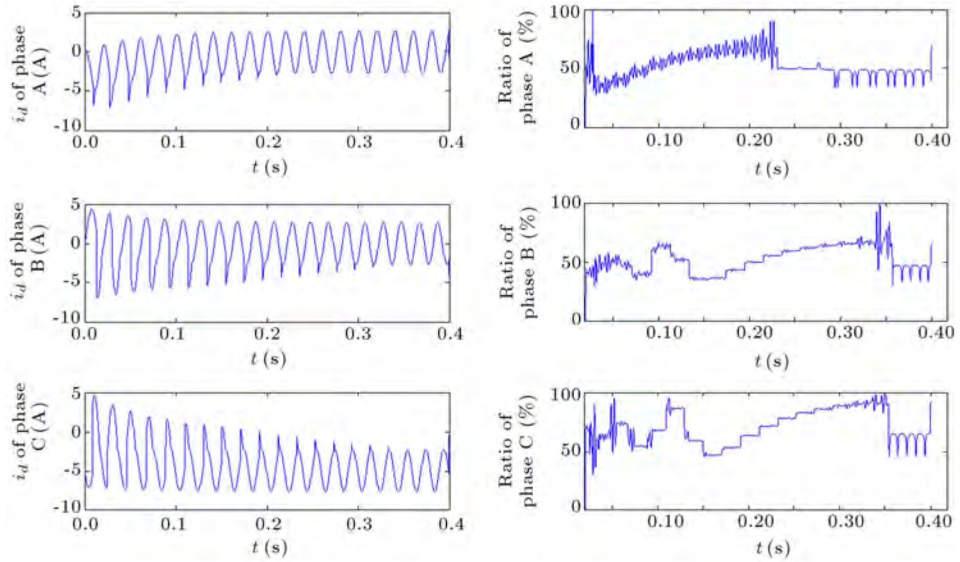

Figure 11d. The differential currents and the ratio of the seventh harmonic to the fifth harmonic of the differential currents due to the ultra-saturation phenomenon under very heavy current transformer saturation.

proposed algorithm, under different conditions, such as different loads (various percentages of nominal load), various inception angles, fault resistance, various residual flux and current transformer saturation (if the resistance component increases in the burden impedance of the current transformer, the distortion will increase in the secondary current of the current transformer and the current transformer is subjected to a high saturation) has been investigated, and under all conditions, the ratio of the seventh harmonic to the fifth harmonic of the differential currents is always higher than 20%, due to the ultra-saturation phenomenon. Furthermore, in the current transformer saturation conditions under inrush current and external faults, the seventh harmonic to the fifth harmonic is higher than threshold value (20%). So, using the proposed algorithm, internal from external faults, the inrush current and the ultra-saturation phenomenon are distinguished and, hence, will prevent the false trip of the differential protection of power transformers.

5. Conclusion

In this paper, at first, a new model for investigating the ultra-saturation phenomenon during the energization of a loaded three-phase power transformer was presented. To model the ultra-saturation phenomenon, the nonlinear characteristics of the transformer core and the saturation effect of the current transformers were taken into account. It was assumed that the load of the transformer is a resistive and inductive load. Also, a new simple and effective model was presented for the current transformer. In this paper, in addition to a new model for the power transformer and the current transformer, a new algorithm for three-phase power transformer differential protection, considering the effect of the ultra-saturation phenomenon, was presented. In this algorithm, the ultra-saturation phenomenon, and the external and internal faults of the power transformer and inrush current were simulated and appropriate criteria using signal harmonic components of the differential current were presented to distinguish between these phenomena using the DFT algorithm. The differential protection of the power transformer must be fast and accurate, so, the description and control of the ultra-saturation phenomenon is necessary for preventing the false trip of the differential protection.

References

1. Mathews, C. "An improved transformer differential relay", *AIEE Trans.*, pt. III, **73**, pp. 645-650 (1954).
2. Specht, T. "Transformer magnetizing inrush current", *AIEE Trans.*, pt. I, **70**, pp. 323-328 (1951).
3. Xiangning, L. and Liu, P. "The ultra-saturation phenomenon of loaded transformer energization and its impacts on differential protection", *IEEE Transactions on Power Delivery*, **20**(2), pp. 1265-1272 (2005).
4. Weng, H., Xiangning, L. and Liu, P. "Studies on the operation behavior of differential protection during a loaded transformer energization", *IEEE Transactions on Power Delivery*, **22**(3), pp. 1386-1391 (2007).
5. Wiszniewski, A., Rebizant, W., Bejmert, W. and Schiel, L. "Ultra saturation phenomenon in power transformers myths and reality", *IEEE Transactions on Power Delivery*, **23**(3), pp. 1327-1334 (2008).
6. Wiszniewski, A., Ungrad, H. and Winkler, W., *Protection Techniques in Electrical Energy Systems*, New York: Marcel Dekker (1995).
7. "Numerical differential protection relay for transformers, generators, motors and mini bus bars", SIEMENS AG, 7UT613/63x V.4.06 Instruction Manual, Order. C53000-G1176-C160-2 (2006).
8. Hossam, A. and Refaey, M. "A novel algorithm for discrimination between inrush current and internal faults in power transformer differential protection based on discrete wavelet transform", *Electric Power Systems Research*, **81**, pp. 19-24 (2011).
9. Gaouda, A. and Salama, A. "DSP wavelet-based tool for monitoring transformer inrush currents andinternal faults", *IEEE Transactions on Power Delivery*, **25**(3), pp. 1258-1267 (2010).
10. Chen, A. and Lin, C., *Fuzzy Approaches for Fault Diagnosis of Transformers, Fuzzy Sets and Systems*, **118**, pp. 139-151 (2001).
11. Naresh, R., Sharma, V. and Vashisth, M. "An integrated neural fuzzy approach for fault diagnosis of transformers", *IEEE Transactions on Power Delivery*, **23**(4), pp. 2017-2024 (2008).
12. Tripathy, M., Maheshwari, R. and Verma, H. "Power transformer differential protection based on optimal probabilistic neural network", *IEEE Transactions on Power Delivery*, **25**(1), pp. 102-112 (2010).
13. Namdari, F., Seifi, H. and Shartash, H. "Digital differential protection of power transformers using artificial neural network", *Iranian Conference on Electrical Engineering* (2001).
14. Mao, P. and Aggarwal, R. "A novel approach to the classification of the transient phenomena in power transformers using combined wavelet transform and neural network", *IEEE Transactions on Power Delivery*, **16**(4), pp. 654-660 (2001).
15. Hamilton, R. "Analysis of transformer inrush current & comparison of harmonic restraint methods in transformer protection", *IEEE Transactions on Industry Applications*, **14**(1), pp. 1876-1884 (2013).
16. Oliveira, L.M.R. and Cardoso, A.J.M. "Extended Park's vector approach-based differential protection of three-phase power transformer", *IET Electric Power Applications*, **6**(8), pp. 463-472 (2012).
17. Zhang, H., Ven, J., Liu, P., Malik, O.P. "Discrimination between fault and magnetization inrush current in transformer using short-time correction transform", *Electrical Power and Energy System*, **24**, pp. 557-562 (2002).
18. Shah, A.M. and Bhalja, B.R. "Discrimination between internal faults and other disturbances in transformer using the support vector machine-based protection scheme", *IEEE Transactions on Power Delivery*, **28**(3), pp. 1508-1515 (2013).
19. Zhang, W., Tan, O., Miao, S., Zhou, L. and Liu, P. "Self-adaptive transformer differential protection", *IET Generation, Transmission & Distribution*, **7**(1), pp. 61-68 (2013).
20. Hoshyar, A., Sanaye-Pasand, M., Afsharnia, S., Davarpanah, M. and Ebrahimi, B.M. "Time-domain analysis of differential power signal to detect magnetizing inrush in power transformer", *IEEE Transaction on Power Delivery*, **27**(3), pp. 1394-1404 (2012).
21. Zheng, T., Gu, J., Huang, S.F., Guo, F. and Terzija, V. "A new algorithm to avoid maloperation of transformer differential protection in substations with an inner bridge connection", *IEEE Transaction on Power Delivery*, **27**(3), pp. 1178-1185 (2012).
22. Gajic, Z. "Use of standard 87T differential protection for special three-phase power transformers - Part II: Application and testing", *IEEE Transaction on Power Delivery*, **27**(3), pp. 1041-1046 (2012).

23. Mozina, C.J. "Protection and commissioning of digital transformer relays: Improvements in medium-voltage industrial transformer protection", *IEEE Industry Applications Magazine*, **18**(6), pp. 63-73 (2012).

24. Barbosa, D., Coury, D.V. and Oleskovicz, M. "New approach for power transformer protection based on intelligent hybrid systems", *IET Generation, Transmission & Distribution,*, **6**(10), pp. 1009-1018 (2012).

25. Pedra, J., Saniz, L., Corcoles, F., Lopez, R. and Salichs, M. "PSPICE computer model of a nonlinear three-phase three-legged transformer", *IEEE Transactions on Power Delivery*, **19**(1), pp. 200-207 (2004).

26. Naidu, M. and Swift, G. "Dynamic analysis of a current transformer during faults", *Electric Power System Research*, pp. 225-231 (1986).

27. Rezaei, A., Iravani, R., Sanaye-Pasand, M., Mohseni, H. and Farhangi, S. "An accurate current transformer model based on Preisach theory for the analysis of electromagnetic transients", *IEEE Transactions on Power Delivery*, **23**(1), pp. 233-242 (2008).

Biographies

Bahram Noshad was born, in 1980, in Marvdasht, Iran. He received a BS degree in Electrical Engineering from Shiraz, Iran, in 2002, an MS degree from the University of Tarbiat Modares, Tehran, Iran, in 2004, and is currently pursuing a PhD degree at Shahid Chamran University (SCU), Tehran, Iran. His areas of interest include operations, power electronics and power system protection.

Morteza Razaz was born in Dezful, Iran, in 1948. He received BS and MS degrees in Electrical Engineering and Applied Mathematics from Texas University, USA, in 1977 and 1979, respectively, and a PhD degree from Sharob University, UK, in 1993. Currently, he is with the Department of Electrical Engineering at Shahid Chamran University, Ahvaz, Iran. His research interests include power electronics, protection relay, and electric machinery.

Seyed Ghodratollah Seifossadat was born in Ahvaz, Iran, in 1963. He received a BS degree in Electrical Engineering from Iran University of Science and Technology (IUST), Tehran, Iran, in 1989, an MS degree in Electrical Engineering from Ferdowsi University of Mashhad, Iran, in 1992, and a PhD degree from IUST, Tehran, Iran, in 2006. Currently, he is in the Department of Electrical Engineering at Shahid Chamran University, Ahvaz, Iran. His research interests are power electronics, protection relay, and electric machinery.